Appl Phys A (2011) 105:125–129
DOI 10.1007/s00339-011-6579-6

Applied Physics A
Materials Science & Processing

Study of femtosecond ablation on aluminum film with 3D two-temperature model and experimental verifications

Qiang Li · Huiying Lao · Jia Lin · Yuping Chen · Xianfeng Chen

Received: 30 May 2011 / Accepted: 17 August 2011 / Published online: 13 September 2011

Abstract In this paper, a 3D two-temperature model is introduced to investigate femtosecond ablation on aluminum film. 3D temperature evolutions for both electrons and lattice are obtained, which present us a vivid view of the energy transformation process during femtosecond ablation. Simulated 3D ablation craters irradiated by a single pulse with different energy are acquired, from which we can easily and precisely predict crater depth and radius before ablation takes place. In the experiment we measure the radii of the craters ablated by pulses with different energy and numbers delivered from a chirped pulse amplification Ti: sapphire system. The threshold fluence for both single and multi pulses are obtained. Comparisons are made between results of the experiment and relative simulated calculations show the reliability of our proposed calculation model.

1 Introduction

With recent progress of laser system, especially that based on the chirped pulse amplification (CPA) technique, ultrafast lasers have been more and more used as a useful tool for different materials processing on the scale of optical wavelength [1–6]. Compared with nano- and pico-second processing, femtosecond processing has the advantages of particular localized material removal and well reduced heat-affected zones [7]. Femtosecond ablation has already shown these advantages in fabricating microstructure in solid targets [1], machining photonic devices [3], writing waveguides [4], manufacturing microfluidic channels [5] and other kinds of precise micromachining [6]. Femtosecond pulses ablation involves many complicated physical processes, including electron and lattice energy absorbing and transportation, electron-phonon energy coupling and accumulation, and a clear understanding of all these would be of great importance for the further development of femtosecond micromachining technology.

During the process of femtosecond ablation, the electron-lattice relaxation time is typically the order of several picoseconds, while the actual laser pulse has a length of only some hundred femtoseconds, hence the material exposed to femtosecond laser pulses gets excited into a high non-equilibrium state, and the classical Fourier heat conduction equation is unavailable in such a highly non-equilibrium state. In order to solve this problem, a two-temperature model (TTM) was proposed [8]. This continuous model describes the energy transfer inside a metal with two coupled generalized heat conduction equations for the temperature of the electrons T_e and the lattice T_l.

In this paper, we introduce a 3D two-temperature model (TTM) to simulate femtosecond ablation on the aluminum film. By using a finite-difference method to solve heat flux equations we obtain the 3D temperature evolution for both electrons and lattice, which presents us a vivid view of the energy transformation process during femtosecond ablation. In order to verify our calculation, the single-pulse experiment is carried out. Craters radii are measured and single-pulse threshold fluence is obtained. Comparisons are made between theoretical analysis and the corresponding experimental results show the feasibility of our 3D two-temperature model. In order to shed light onto multi-shot ablation, multi-pulse experiment is also conducted and the result is also discussed in this paper.

Q. Li · H. Lao · J. Lin · Y. Chen · X. Chen (✉)
Department of Physics, Key Laboratory for Laser Plasmas (Ministry of Education), Shanghai Jiao Tong University, Shanghai 200240, China
e-mail: xfchen@sjtu.edu.cn

2 Modeling and discussion

The well-known two-temperature model (TTM) originally proposed by Anisimov et al. is presented as follows [8]:

$$C_e \frac{\partial T_e}{\partial t} = \nabla(k_e \nabla T_e) - G(T_e - T_l) + Q, \tag{1}$$

$$C_l \frac{\partial T_l}{\partial t} = G(T_e - T_l) \tag{2}$$

Here $C_e = kT_e$ and k_e are the thermal capacity and thermal conductivity of electrons respectively; C_l is the lattice heat capacity, which we take as a constant; G is the electron-phonon coupling coefficient, and $Q(x, y, z, t)$ is the laser heating source term which can be described by

$$Q(x, y, z, t) = S(x, y, z) \bullet T(t), \tag{3}$$

$$S(x, y, z) = \frac{1 - R}{\delta + \delta_b} F \bullet \exp\left(-\frac{z}{\delta + \delta_b} - \frac{(x - x_0)^2 + (y - y_0)^2}{w_0^2}\right), \tag{4}$$

$$T(t) = \frac{1}{t_p}\sqrt{\frac{4\ln 2}{\pi}} \exp\left(-4\ln 2\left(\frac{t - 2t_p}{t_p}\right)^2\right) \tag{5}$$

Here, R is the reflectance of the target; δ is the optical penetration of aluminum film and δ_b is the ballistic length; F is the laser fluence; x_0 and y_0 are the x-coordinate and y-coordinate of the laser spot center, respectively; w_0 is $1/e$ radius of the laser spot and t_p the FWHM pulse duration.

As the ablation process takes place on a timescale of several picoseconds, it is reasonable to ignore the heat losses from the metal film to the surrounding and to the front surface during the ablation process, so the boundary condition can be given by [9]

$$T_e(x, 0) = T_l(x, 0) = T_0, \tag{6}$$

$$\left.\frac{\partial T_e}{\partial n}\right|_{x=0} = \left.\frac{\partial T_e}{\partial n}\right|_{x=d} = 0 \tag{7}$$

where T_0 is the original temperature of the aluminum film; d is the thickness of the target.

We use the finite-difference method to solve (1) and (2). A time step of 10 fs, an x–y plane step of 0.1 μm and a z direction step of 1 nm (x–y plane is perpendicular and z axis parallel to the laser direction) are used in the simulation. The relative physical parameters of aluminum and the laser used in numerical simulation are given as follows:

$k_e = 235$ J/(mK s), $k = 134.5$ J/(m^3 K^2),

$G = 5.69 \times 10^{17}$ J/(m^{3}K s), $C_l = 2.42 \times 10^6$ J/(m^3 K),

$R = 0.88$, $\delta = 20$ nm, $\delta_b = 100$ nm, $T_0 = 300$ K,

$t_p = 100$ fs, $w_0 = 12.4$ μm

Figure 1 gives the simulated results of the electrons and lattice temperature evolution for both x–y and x–z plane. The energy fluence F here is taken to be 1 J/cm^2. We can see that at the time 10 fs, both the electrons and the lattice are still quite cool, while at the time 100 fs the electrons are quickly overheated with a temperature higher than 15000 K in the center of the front surface. In contrast, the lattice still keeps cool with a temperature nearly the same as room temperature. This clearly shows us that laser energy is first absorbed by the electrons. As time goes on, the electrons' temperature drops while the lattice temperature spreads further and penetrates deeper into the target. So during this period laser energy is transformed from the high temperature electrons to the lattice. At the time of about 5 ps the two temperatures are approximately the same and the target keeps being thermal equilibrious from that time on.

Knowing the three-dimension temperature evolution of the target means that we can precisely predict the shape of ablation hole before ablation take place, which would be of directive significance to femtosecond micromachining technology. It is well known that during the ablation process, when the temperature of the lattice reaches the thermodynamic critical temperature T_c (for aluminum it is 5720 K), such a high temperature would inevitably lead to an extremely high pressure in the ablated region, and such a great pressure will be released through the adiabatic expansion, which would finally lead to obvious material ablation and ejection [10]. In the actual calculation $0.9T_c$ is always set as the critical temperature for material removal during femtosecond ablation [11]. Figure 2 presents simulated ablation craters by single pulse with different energy. It can be seen from Fig. 2a, b, and c that with the increase of pulses energy fluence, there is an obvious increase in the ablation depth. Crater depths ablated by pulses with different energy fluence are given in Fig. 3. We can obviously see that when the fluence is low there is a logarithmic dependence, whereas in the high-fluence regime the dependence turns into linear. This is because in the low-energy fluence region heat propagation is weak and can be neglected while in the high-energy fluence region heat propagation becomes significant. This phenomenon is already well studied and explained by other works [12]. From Fig. 3 we can see that ablation depth $h > 0$ only when pulses energy fluence $F > 0.9$ J/cm^2 and when $F \leq 0.9$ J/cm^2 the crater depth equals zero. This result obviously shows us that the threshold fluence for aluminum is 0.9 J/cm^2 in our simulation, which is pretty much the same as other reports [13].

3 Experimental results and discussions

The laser used in our experiment is a standard Ti:Sapphire system comprising an oscillator (Coherent, model Mira

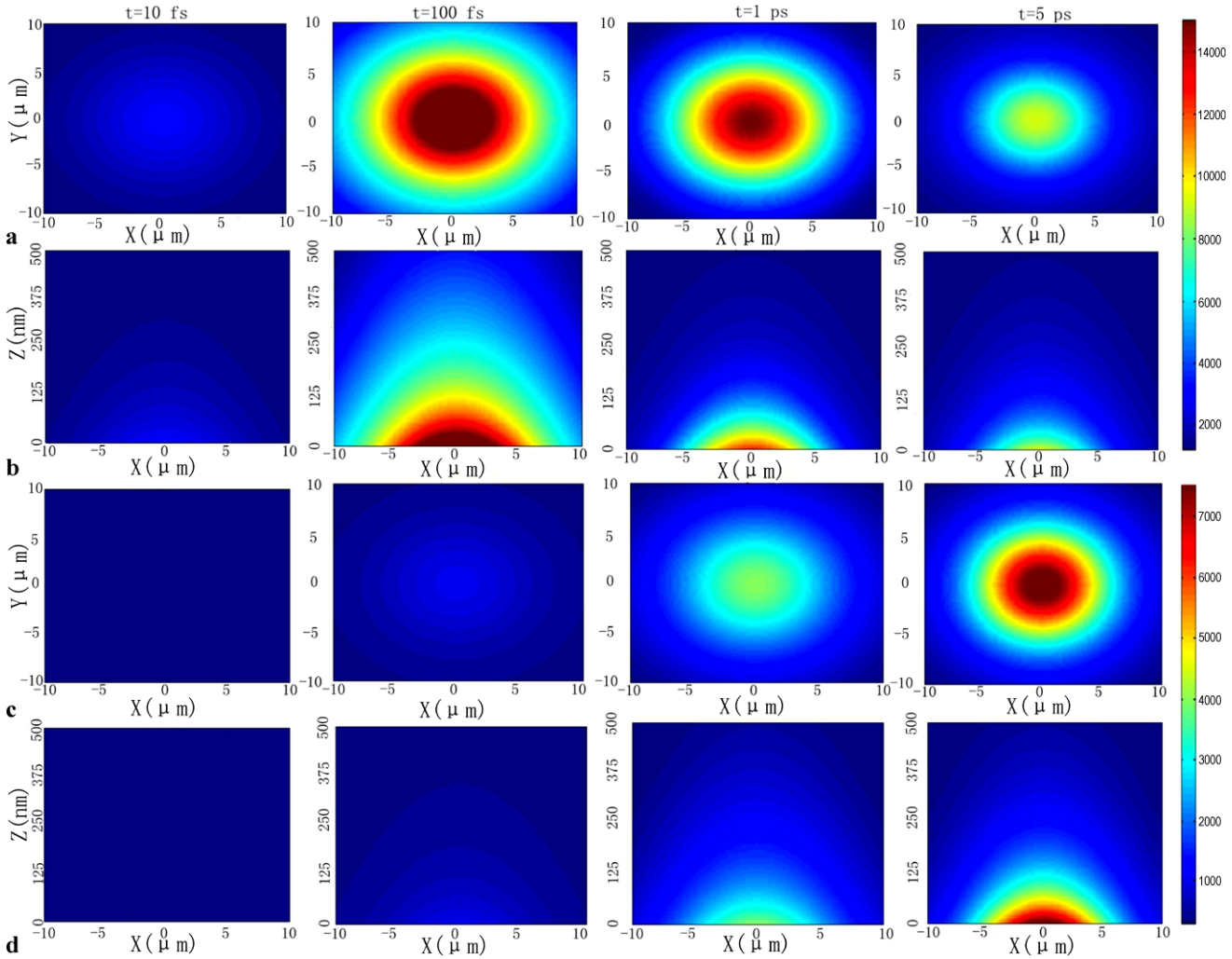

Fig. 1 Temperature evolution for electrons and lattice of both $x-y$ plane and $x-z$ plane. (**a**) T_e, $x-y$ plane (**b**) T_e, $x-z$ plane (**c**) T_l, $x-y$ plane (**d**) T_l, $x-z$ plane

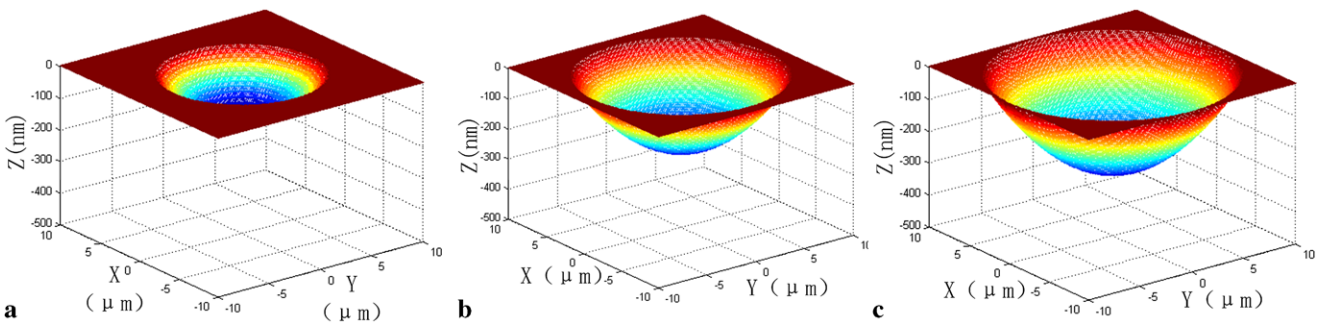

Fig. 2 Simulated 3D ablation craters by single pulses with different energy fluence. (**a**) 2 J/cm^2 (**b**) 5 J/cm^2 (**c**) 8 J/cm^2

900F) and an amplifier (Coherent, model Legend). The amplified pulses are of 100 fs duration at a central wavelength of 800 nm and the repetition rate of the laser is 1 kHz. The aperture is used to optimize the shape of laser spot and a rotatable half-wave plate followed by a polarizer to change the energy of laser pulses. In order to get the desired number of pulses, a speed-controllable mechanical shutter is used. The beam is finally focused onto the sample using a 20× objective lens. The sample is fixed onto a motor-controlled XYZ stage with a resolution of 0.4 μm and the film is positioned

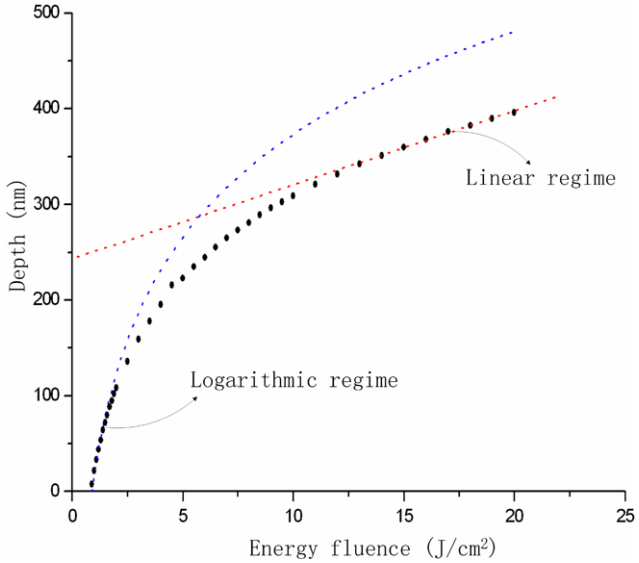

Fig. 3 Depth of simulated ablation craters versus laser pulse energy fluence

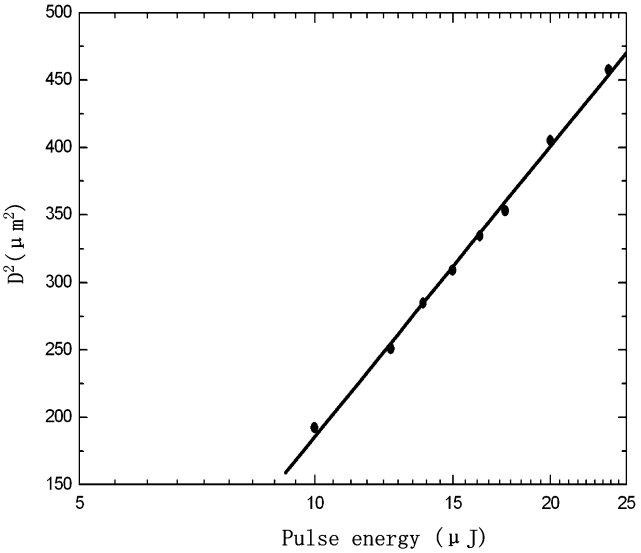

Fig. 4 Ablation craters diameters squared versus the pulses energy for single pulse

in the way that its surface is perpendicular to the direction of the incident laser beam. A CCD is used to monitor the ablation process.

For a Gaussian spatial beam profile with a $1/e^2$ laser beam radius w_0, the spatial distribution of the laser fluence can be expressed by

$$F(r) = F_0^{\mathrm{p}} \exp\left(-\frac{2r^2}{w_0^2}\right) \tag{8}$$

Here F_{p} represents the peak laser fluence and r is the distance to the center of the laser spot; F_{th} represents the ablation threshold fluence, which means that when $F \leq F_{\mathrm{th}}$, the crater diameter D equals zero. We obtain [14]

$$D^2 = 2w_0^2 \ln\left(\frac{F_0^{\mathrm{p}}}{F_{\mathrm{th}}}\right) \tag{9}$$

The laser peak fluence can be calculated by using single-pulse energy E and laser focus radius by the following equation:

$$F_0^{\mathrm{p}} = \frac{2E_{\mathrm{pulse}}}{\pi w_0^2} \tag{10}$$

From (8) and (9) we have

$$D^2 = 2w_0^2 \ln\left(\frac{E_{\mathrm{pulse}}}{E_{\mathrm{th}}}\right) \tag{11}$$

Figure 4 shows the measured fluence dependence of the squared diameter of ablated area under single shot. The dots give our experimental results and the solid line represents a least square fit to (10) and each of the dots in Fig. 1 represents one individual shot of our experiment. The diameter of the ablated craters is found by a scanning electron microscope (SEM) which has a precision of 0.01 μm. The laser used in our experiment has a very stable output, with each pulse of nearly the same energy, so we obtain the energy of each single pulse by measuring the power of the laser and then use the repletion rate to divide it. The power meter in our experiment has a precision of 0.01 mW and it means that our measurement of the pulse energy has an accuracy of 0.01 μJ. From the slope of the line we can get $w_0 = 12.4$ μm. By extrapolating the fitted line to $D^2 = 0$, the single-pulse threshold is found to be $F_{\mathrm{th}} = 1.12$ J/cm^2, which is little higher than our theoretical calculation (0.9 J/cm^2). Considering that our experiment is carried out in air while our simulation is in vacuum environment, and it is reported that metal ablation in air is significantly less efficient than in vacuum due to redeposition of ablated material [15], it is quite reasonable to say that our experimental result fits very well with our calculation.

In order to gain insight into multi-shot ablation, which is of great importance to both scientific research and industry processing, multi-shot ablation experiments are carried out. Crater diameters ablated by pulses with different energy and numbers are measured and the result is shown by Fig. 5. The dots signify our experimental results and the solid lines represent the least square fits to (10). Taking errors of measurement into consideration, the fit lines are parallel to each other. By extrapolating the fitted lines to $D^2 = 0$ we can obtain the threshold fluence for different pulses number. Figure 6 presents the result. We can see that with the increase of the pulse number the ablation threshold fluence decreases. This is also reported by studies on other kinds of material and can be explained by the so-called incubation effect. We use the equation $F_{\mathrm{th}}(N) = F_{\mathrm{th}}(1) \cdot S^{N-1}$ which was first pro-

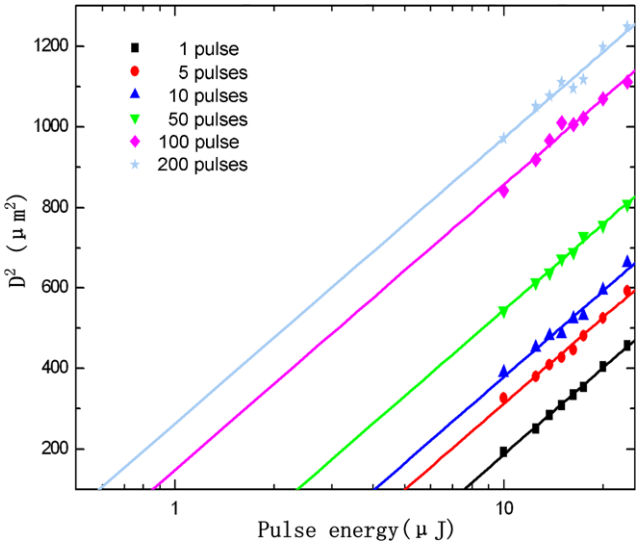

Fig. 5 Ablation craters diameters squared versus the pulse energy for different pulses

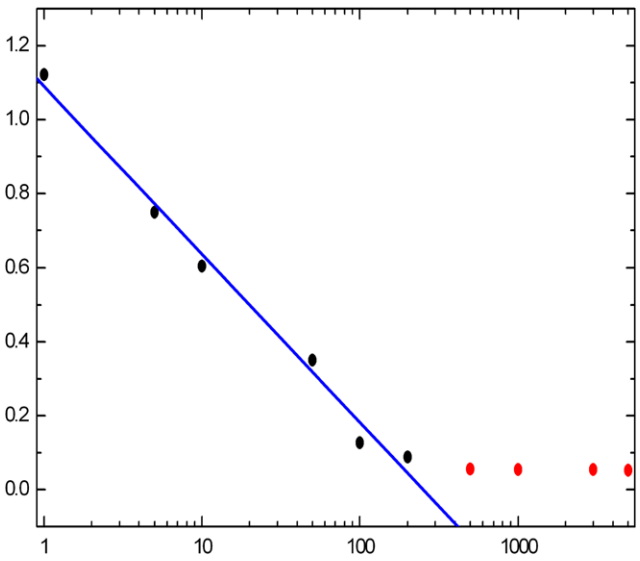

Fig. 6 Threshold fluence for different pulse numbers

posed by Jee et al. [16] to fit the experimental data. The parameter S is the so-called incubation coefficient, which quantifies the degree of incubational behavior. The solid line in Fig. 6 gives the least square fit. We can see that when N is relatively small the equation fits quite well, but when N is large (in our experiment, that is, above 200) there is an obvious deviation between the equation and the result of the experiment. This means that the incubation effect is only limited to a certain number of pulses, and beyond that certain number (in our experiment it is 200 for the aluminum film) the incubation effect becomes saturated and the ablation threshold fluence keeps nearly unchanged even as the pulse number increases.

4 Conclusion

In conclusion, we have introduced a 3D TTM to investigate femtosecond ablation on an aluminum film. The energy transportation process is clearly and vividly demonstrated. 3D craters ablated by single pulses with different energy fluence are simulated, from which we can simply predict the radii and depths of ablation holes before ablations take place. This would be of instructive significance to femtosecond ablation technology. In our experiment we measured radii of craters ablated by single femtosecond pulses with different energies and calculated the single-shot ablation fluence from the data of the experiment. The result of the experiment fits quite well with our simulation. In the multi-pulse experiment we observe an obvious incubation effect of the ablation threshold fluence for aluminum. We also discover that the incubation effect limits to only a certain number of pulses and beyond that number the incubation effect becomes saturated.

Acknowledgements This research was supported by the National Natural Science Foundation of China (61078009 and 10874121), the National Basic Research Program "973" of China (2011CB808101).

References

1. S. Nolte, C. Momma, H. Jacobs, A. Tünnermann, B. Chichkov, B. Wellegehausen, H. Welling, J. J. Opt. Soc. Am. B, Opt. Phys. **14**, 2716 (1997)
2. S. Kawata, H.B. Sun, T. Tanaka et al., Nature **412**, 697 (2001)
3. K. Minoshima, A.M. Kowalevicz, E.P. Ippen, J.G. Fujimoto, Opt. Express **29**, 645 (2002)
4. A. Benayas, W.F. Silva et al., Opt. Lett. **35**, 330 (2010)
5. Y. Liao, Y. Ju, Y. Cheng et al., Opt. Lett. **35**, 3225 (2010)
6. H. Lao, H. Zhu, X. Chen, Appl. Phys. A **101**, 313 (2010)
7. B.N. Chichkov, C. Momma, S. Nolte, F. von Alvensleben, A. Tünnermann, Appl. Phys. A **63**, 109 (1996)
8. S.I. Anisimov, B.L. Kapeliovich, JETP Lett. **39**, 375 (1974)
9. G. Du, F. Chen, Q. Yang, J. Si, X. Hou, Opt. Commun. **283**, 1869 (2010)
10. N. Zhang, X. Zhu, M. Wang et al., Phys. Rev. Lett. **99**, 167602 (2007)
11. J. Kim, S. Na, Opt. Laser Technol. **39**, 1443 (2007)
12. J. Byskov-Nielsen, J.-M. Savolainen, M.S. Christensen, P. Balling, Appl. Phys. A **101**, 97 (2010)
13. W. Perrie, A. Rushton, M. Gill, P. Fox, W. O'Neill, Appl. Surf. Sci. **248**, 213 (2005)
14. J. Kim, S. Na, Opt. Laser Technol. **39**, 1443 (2007)
15. S. Preuss, A. Demchuk, M. Stuke, Appl. Phys. A **61**, 33 (1995)
16. Y. Jee, M.F. Becker, R.M. Walser, J. Opt. Soc. Am. B **5**, 648 (1988)